ORGANIC CHEMISTRY FRONTIERS

RESEARCH ARTICLE

View Article Online
View Journal | View Issue

Cite this: *Org. Chem. Front.*, 2022, **9**, 1649

Chiral *N*-triflylphosphoramide-catalyzed asymmetric hydroamination of unactivated alkenes: a hetero-ene reaction mechanism†

Na Wang,[a,b,c] Li-Wen Fan,[c] Jin Zhang,[c] Qiang-Shuai Gu,[d] Jin-Shun Lin,[c] Guo-Qiang Chen,*[a] Xin-Yuan Liu *[c] and Peiyuan Yu *[c]

A highly enantioselective intramolecular hydroamination reaction catalyzed by chiral *N*-triflylphosphoramide (NTPA) that features an exceptionally broad substrate scope of isolated unactivated alkenes was recently reported by some of us. Herein we report a detailed density functional theory (DFT) study that unveil an uncommon hetero-ene reaction mechanism for this transformation. The reaction changes from a stepwise mechanism involving discrete tertiary carbocation formation to a concerted mechanism to avoid the generation of energetically unfavorable secondary carbocation species for distinctly substituted alkene substrates. The reactivity of this reaction is primarily affected by the substituents on the internal carbon of the alkene, with the carbocation-stabilizing ones promoting the reaction. In addition, the reaction is also influenced by the substituents on the terminal alkene carbons: those diminishing the innate alkene polarization of the starting alkenes retard the reaction by disfavoring the formation of related transition states featuring highly polarized alkene residues. The steric effect of all these alkene substituents was found to be largely unimportant due to the unique arrangement of the hetero-ene reaction complex that keeps the reacting alkene away from the sterically congested core region of the catalyst pocket. The lower acidity of chiral phosphoric acids than that of chiral NTPAs renders the protonated precomplex along the hetero-ene reaction pathway greatly thermodynamically disfavored. This indirectly results in a greater relative distortion in the corresponding transition state, which in turn causes reaction retardation. Our results demonstrate the use of intramolecular pericyclic reactions as an alternative strategy for alkene activation by chiral Brønsted acid catalysis and provide insights into the further development of asymmetric hydrofunctionalization of unactivated alkenes.

Received 17th December 2021,
Accepted 2nd February 2022

DOI: 10.1039/d1qo01874d

rsc.li/frontiers-organic

Introduction

The direct 1,2-hydrofunctionalization of alkenes with an inter- or intramolecular pronucleophile (H–Nu) represents a robust and versatile synthetic tool in organic synthesis, thanks to the inherently high atom-economy and the readily available starting materials.[1,2] Thus, tremendous efforts have been made to develop a variety of catalytic systems for this type of reaction,[1] particularly those delivering valuable enantioenriched products.[1a,c,e,f] Among others, Brønsted acids[3] have long been known to activate alkenes *via* direct protonation for further functionalization (Scheme 1a).[4] However, isolated unactivated alkenes constitute a great challenge for this type of activation due to their inherently unpolarized double bonds and low-lying highest-occupied molecular orbitals (HOMO). Accordingly, either extremely high reaction temperatures[5] or very strong Brønsted acids[4b,c,6] are generally necessary for bringing about the hydrofunctionalization of these alkenes, which undesirably limits the synthetic value and renders the development of the corresponding enantioselective variants challenging.[5a] In this aspect, Yamamoto *et al.* have pioneered the use of Lewis acid-assisted Brønsted acid (LBA) catalysts for achieving highly enantioselective intramolecular polyene-cyclization.[7] Later, Ishihara *et al.* used chiral Lewis base-assisted Brønsted acid (LBBA) catalysts for achieving the same type of polyene-cyclization as well as an enantioselective intramolecular hydrocarboxylation reaction.[8] Recently, List *et al.*

[a]*College of Chemistry and Environmental Engineering, Shenzhen University, Shenzhen 518071, China. E-mail: gqchen@szu.edu.cn*
[b]*College of Physics and Optoelectronic Engineering, Shenzhen University, Shenzhen 518060, China*
[c]*Department of Chemistry and Shenzhen Grubbs Institute, Guangdong Provincial Key Laboratory of Catalysis, Southern University of Science and Technology, Shenzhen 518055, China. E-mail: liuxy3@sustech.edu.cn, yupy@sustech.edu.cn*
[d]*Academy for Advanced Interdisciplinary Studies and Department of Chemistry, Southern University of Science and Technology, Shenzhen 518055, China*
†Electronic supplementary information (ESI) available. See DOI: 10.1039/d1qo01874d

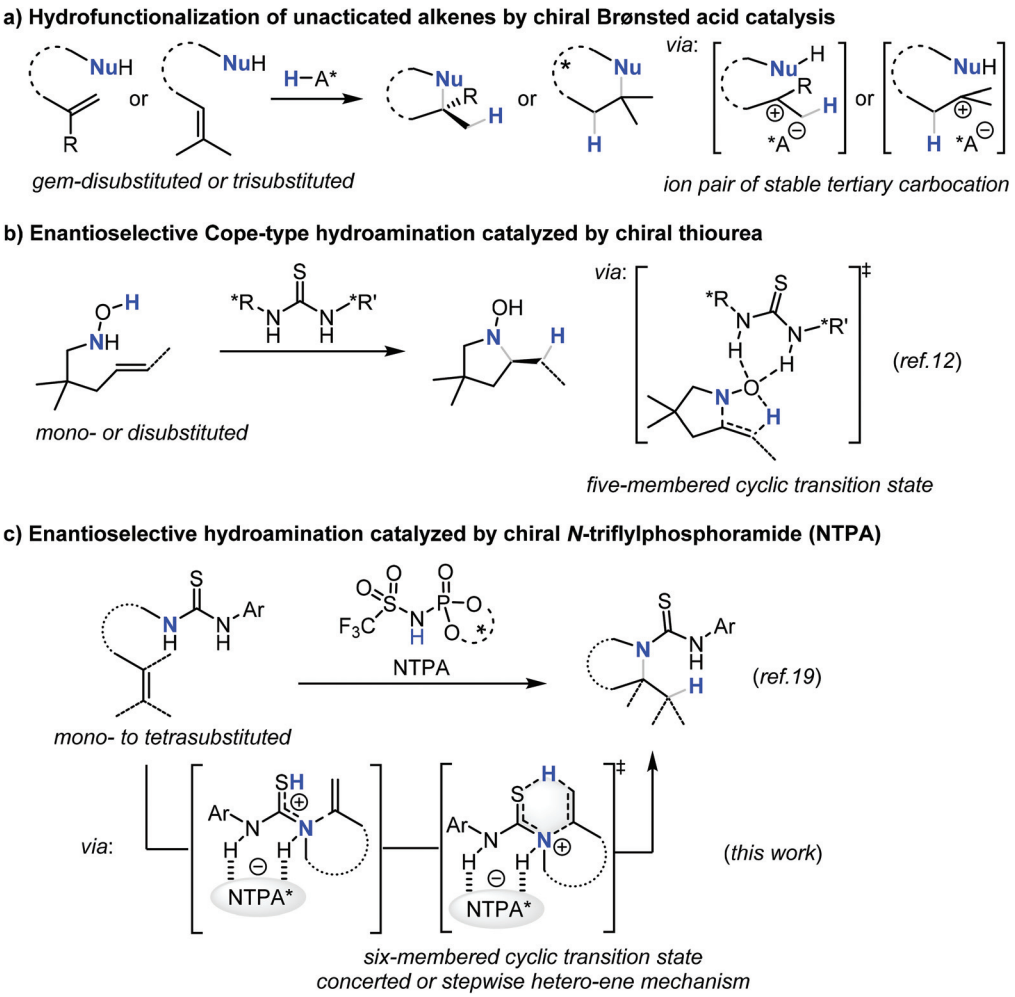

Scheme 1 Enantioselective 1,2-hydrofunctionalization of unactivated alkenes by Brønsted acid catalysis or hydrogen-bond catalysis.

made a breakthrough in this field by accomplishing the enantioselective intramolecular hydroalkoxylation and hydroindolylation reactions using the strong and confined imidodiphosphorimidate (IDPi) Brønsted acid catalysts that they had developed, without any other promoter.[9] While significant progress has been made in this field, these reactions still require either trisubstituted[7,8] or geminally disubstituted[9a,b] alkenes (Scheme 1a),[10] which upon protonation lead to the formation of relatively stable tertiary carbocation species.[11] To the best of our knowledge, isolated monosubstituted and 1,2-disubstituted alkenes that would form unstable secondary carbocation species after conceivable protonation have so far remained largely out of reach for chiral Brønsted acid catalysis.

On the other hand, Jacobsen *et al.* reported an enantioselective intramolecular hydroamination reaction using chiral thiourea hydrogen-bond catalysis (Scheme 1b).[12–14] The reaction proceeds *via* a concerted Cope-type reaction mechanism[15] that is able to avoid the formation of unstable secondary carbocation species.[16] Thus, monosubstituted alkenes were well accommodated in this reaction. However, isolated unactivated multi-substituted alkenes seemed to be incompatible with the reaction, possibly due to the sensitivity of this type of reaction toward steric bulkiness.[17]

Recently, some of us reported enantioselective intramolecular hydroamination[18] reactions catalyzed by chiral *N*-triflylphosphoramide (NTPA) catalysts (Scheme 1c).[19,20] In contrast to the two types of reactions discussed above,[7,8,9a,b,12] these reactions display a surprisingly high tolerance towards alkenes ranging from monosubstituted to tetrasubstituted ones.[19a,c] This prompted us to carry out a detailed theoretical investigation[20,21] in order to delineate the origin for this remarkably broad substrate scope. The results, as discussed in detail below, indicate a rare hetero-ene reaction mechanism that is efficiently promoted by chiral *N*-triflylphosphoramide catalysts.[22]

Computational details

Density functional theory (DFT) computations were performed using Gaussian 16.[23] Conformational searches were initially carried out using Grimme's programs xTB 6.3 and CREST

2.10.2.[24] Next, geometry optimizations were conducted using the B3LYP functional[25] with the 6-31G(d) basis set. Frequency calculations were then performed at the same level of theory to ensure the stationary points as saddle points (one imaginary frequency) or local minima (no imaginary frequency), and to generate thermal corrections at 298 K. Further single-point energy calculations were executed using the M06-2X functional[26] with the 6-311+G(d,p) basis set. The SMD model[27] was employed to take the solvent effects of dichloromethane into consideration. Additional calculations were also performed on the key enantio-determining transition states for compound **AT-1** with B3LYP-D3(BJ),[28] M06-2X,[26] or ωB97X-D[29] density functionals for comparison purposes. All these functionals afforded correct prediction of the major enantiomer while B3LYP and ωB97X-D provided stereoselectivities very close to the experimentally observed ones. The detailed results of the calculations using functionals other than B3LYP are provided in the ESI.† Non-covalent-interaction (NCI) analysis[30] was performed using Multiwfn[31] and the results were visualized using PyMOL.[32] Fragment distortion and interaction energies[33] were calculated at the M06-2X/6-311+G(d,p) level using the B3LYP/6-31G(d) geometries in the gas phase. Natural population analysis (NPA) was performed at the B3LYP/6-31G(d) level using the program NBO 3.0[34] as implemented in Gaussian 16. Molecular structures were visualized using CYLview.[35]

Results and discussion

Model studies on the styrene-type substrate

We started our investigation by using **NTPA-1** and **AT-1** as the model catalyst and substrate, respectively, to identify favorable activation modes of reaction (Fig. 1a). We considered two main activation modes based on the common bifunctional mode for Brønsted acid catalysis[1c,4d] as well as our original proposal[19a] (Fig. 1b). Mode-1 involves the direct alkene protonation by the catalyst, which is assisted by the thiourea moiety of the substrate *via* forming a hydrogen bond with the catalyst. Mode-2 entails alkene protonation by the distal N–H bond of the substrate while the thiourea moiety is activated *via* the protonation or formation of hydrogen bonds with the catalyst. Within each of the two reaction modes, we further considered two additional tautomers of **NTPA-1**, *i.e.*, **NTPA-1′** and **NTPA-1″** (Fig. 1c, left and middle),[36] and two alternative basic sites of the thiourea group (Fig. 1c, right) for possible protonation or forming hydrogen bonds. Accordingly, we systematically evaluated a number of possible combinations and ultimately found that transition states belonging to Mode-1 were generally much more energetically favorable than those belonging to Mode-2 (*e.g.*, **TS-1-1** *vs.* **TS-2-1**, Fig. 1d). Interestingly, while investigating the first reaction mode, we observed facile protonation of the thiourea group by the catalyst, leading to the thermodynamically more stable intermediate **INT-1** (Fig. 1e). The salient isothiourea-like structural characteristic of this complex reminded us of the well-known Conia-ene[37] and ene[38] reactions, which prompted us to investigate the possibility of a heteroatomic variant[39] of such reactions during the hydroamination process. Subsequently, we successfully located one transition state **TS-E-1** (Fig. 1e) along the envisioned hetero-ene reaction pathway, which leads to a carbocation intermediate **INT-2**. The ensuing C–N bond formation occurred without any hindrance (**INT2** to **INT-3** without a locatable transition state) and the final proton transfer was also facile (**INT-3** to **1** *via* the transition state **TS-PT-1** with a barrier of 2.7 kcal mol^{-1}). Overall, this reaction pathway involved a stepwise hetero-ene reaction, which proved to be the most energetically favorable in this model system (at least 1.0 kcal mol^{-1} lower in barrier).

Enantioselective hydroamination of the styrene-type substrate

With the favorable reaction pathways identified using the model catalyst, we next studied the enantioselective hydroamination reaction of styrene-type substrate **AT-1** with the full catalyst **NTPA-2R** (Fig. 2a).[19a] On the basis of the model studies discussed above, we focused on the least energetically demanding hetero-ene reaction pathway as well as on other pathways with relative barriers within 10 kcal mol^{-1}. Our calculations indicate a thermodynamically comparable thiourea protonation for the formation of the pre-TS complex (**INT-4** in Fig. S4b,† $\Delta G = -1.5$ kcal mol^{-1}). The transition state **TS-EF-1S** along the hetero-ene reaction pathway (Fig. 2b) is still energetically lower than all others investigated (at least 2.2 kcal mol^{-1} higher, see Fig. S6† for details). Notably, this transition state features a hydrogen bonding interaction between the triflyl moiety of the catalyst and the urea N–H of the substrate in addition to that of the commonly used phosphoramide group. This result is consistent with previous computational studies,[36] all of which point to the important but often overlooked non-spectator role of the triflyl moiety in NTPA catalysis.[21b] The transient carbocation intermediate **INT-5** undergoes C–N bond formation without any hindrance to afford **INT-6**, which is followed by facile proton transfer to afford the final hydroamination product (Fig. S4b†). Overall, the calculations indicate that the hetero-ene reaction took place in a stepwise manner, with the protonation of the alkene by the thiourea being the rate-limiting ($\Delta G^{\ddagger}$ = 15.3 kcal mol^{-1} for **TS-EF-1S**) and enantio-determining step. Notably, the transition state **TS-EF-1S** was more stable than **TS-EF-1R** by 2.0 kcal mol^{-1}, corresponding to a predicted ee of 93% at room temperature that is comparable to the experimentally observed one (94% ee at 0 °C).[19a] Further distortion/interaction analysis[33] indicated that the selectivity mainly originates from the differences in the distortion energies of the two transition states, which are partially set off by the differences in the interaction energies (Fig. 2c, left). Additional analysis of the substrate and the catalyst fragments, respectively, revealed comparable substrate distortion but quite different catalyst distortion (Fig. 2c, right). Superimposing the catalyst fragments in these two transition states with the corresponding fully relaxed free structure, respectively, unearthed remarkable deviations of one 9-anthranyl group as well as the triflyl moiety in **TS-EF-1R** (Fig. 2d and S8†). Apparently, the triflyl moiety rotates counterclockwise away from its favored position in the fully relaxed free catalyst

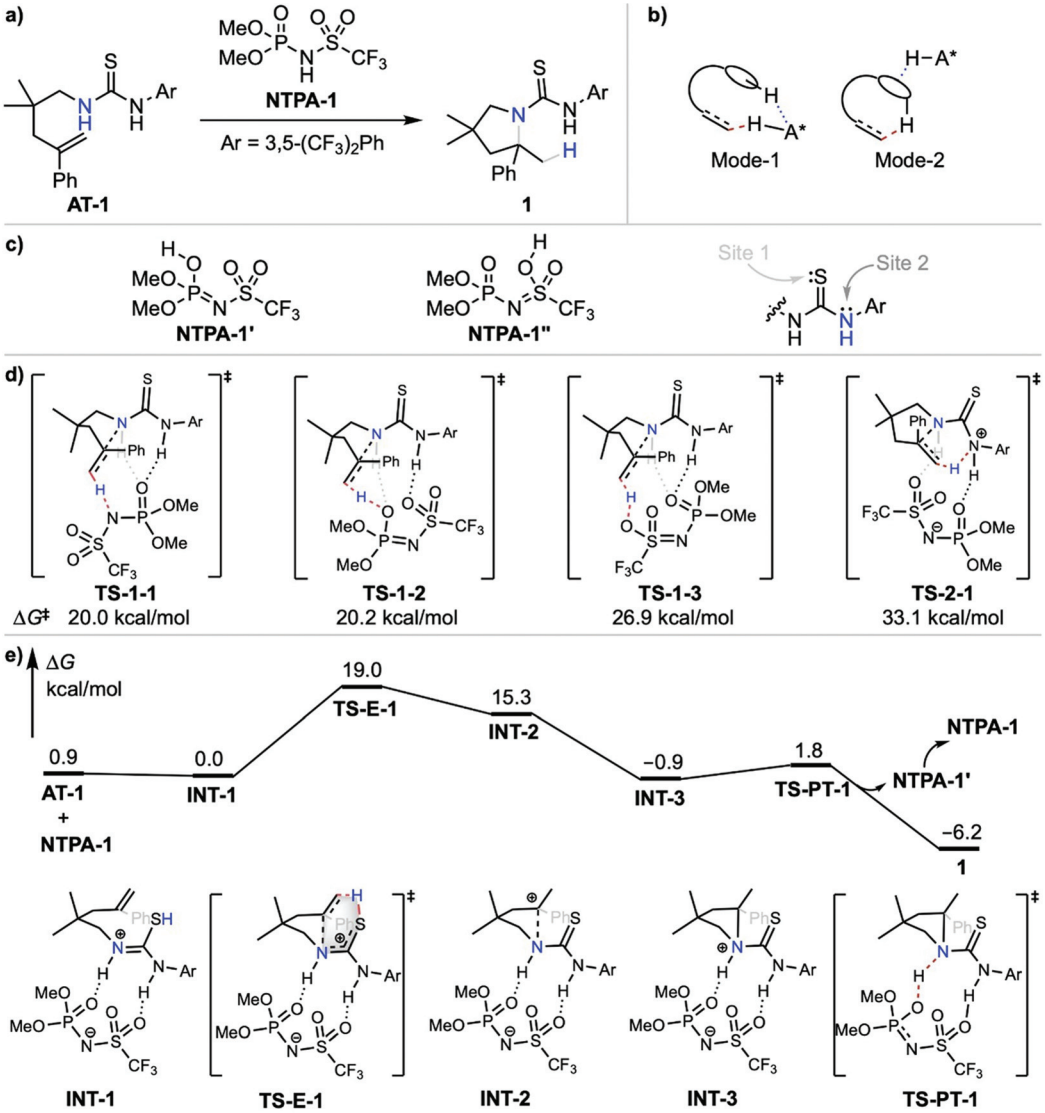

Fig. 1 Model computational study. (a) The hydroamination reaction of **AT-1** catalyzed by model catalyst **NTPA-1**. (b) Two main alkene activation modes. (c) Two additional tautomers of **NTPA-1** and two alternative sites of the thiourea moiety for protonation/hydrogen bonding considered in this study. (d) Computed favorable transition states belonging to Mode-1 and Mode-2 with corresponding activation energies $\Delta G^{\ddagger}$ shown in kcal mol^{-1}. (e) Free energy profile of the hetero-ene reaction pathway.

structure in order to form comparable hydrogen bonding interactions in **TS-EF-1R** to those in **TS-EF-1S.** At the same time, the 9-anthranyl group on the right-hand side of the catalyst rotates clockwise so that the styrene fragment of the substrate in **TS-EF-1R** can be accommodated in the upper right quadrant, as shown in Fig. 2d.

Enantioselective hydroamination of the isolated monosubstituted substrate

Compared to the styrene-type substrate, the protonation of an isolated monosubstituted alkene would lead to the formation of an unstable secondary carbocation species, rendering the corresponding Brønsted acid-catalyzed hydrofunctionalization more challenging. We next took a detailed look at the reaction mechanism for the enantioselective hydroamination of **AT-2** bearing an isolated monosubstituted alkene moiety (Fig. 3a).[19a] Similarly, we found the hetero-ene reaction pathway (Fig. 3b) had the lowest energy (ΔG_{act} = 20.7 kcal mol^{-1}). It is noteworthy that this time we failed to locate a carbocation intermediate like **INT-2** or **INT-4** for the styrene-type substrate **AT-1** during the hetero-ene reaction, which renders the hetero-ene reaction a concerted process. Although significant asynchronicity in the transition states **TS-EF-2S** (C1–H, 1.32 Å; C2–N1, 2.76 Å; Fig. 3c, left) and **TS-EF-2R** (C1–H, 1.34 Å; C2–N1, 2.62 Å; Fig. 3c, right) was observed, the C–N distances are now shorter than those in the stepwise TSs (2.9–3.1 Å) of the styrene-type substrate. The following proton transfer step *via* **TS-PT-3** was still very fast (ΔG_{act} = 4.5 kcal

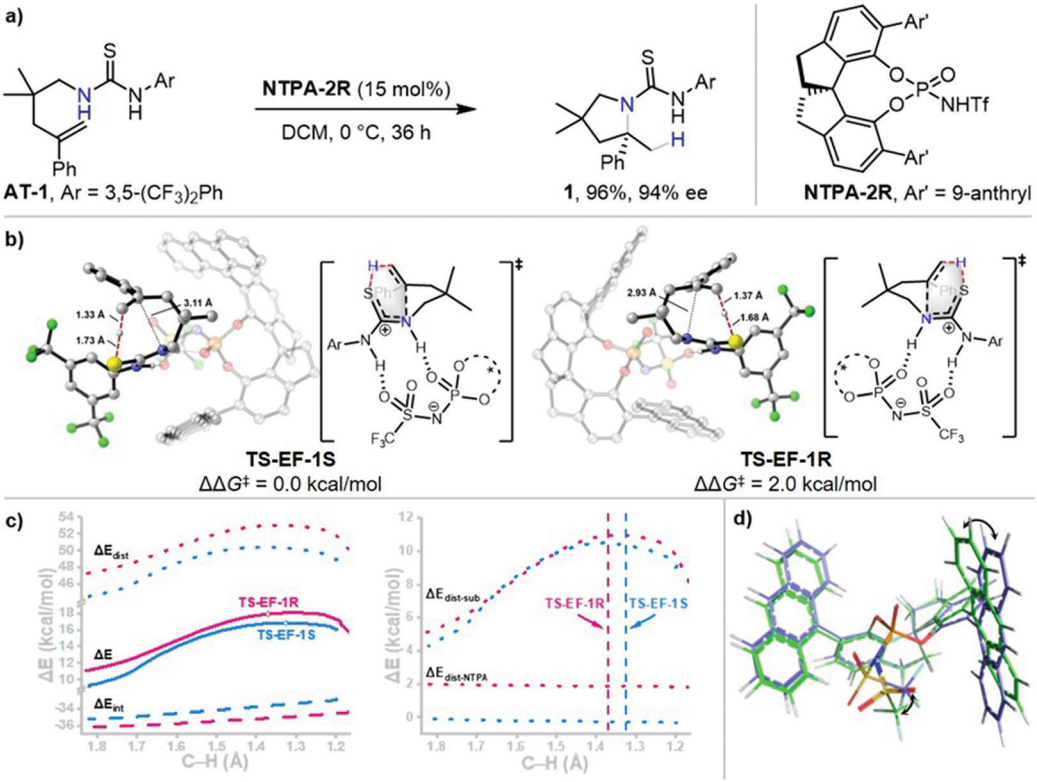

Fig. 2 Computational study on the hydroamination reaction of **AT-1** catalyzed by full catalyst **NTPA-2R**. (a) Experimental results of the hydroamination reaction of **AT-1** catalyzed by **NTPA-2R**. (b) Geometries and energies of the two optimized hetero-ene transition states leading to the two enantiomers of product **1**, respectively. (c) Distortion/interaction analysis on the enantioselective hetero-ene reaction step. (d) Superimposition of the catalyst fragment in **TS-EF-1R** with the corresponding fully relaxed free structure. Carbons in the fully relaxed free structure are drawn in green while that in **TS-EF-1R** purple.

mol^{-1}) and the hetero-ene reaction was the rate-limiting and enantio-determining step. Accordingly, a difference of 1.9 kcal mol^{-1} in free energies of transition states **TS-EF-2S** and **TS-EF-2R** agrees well with the experimentally observed 82% ee.[19a] Additional distortion/interaction analysis of these two transition states (Fig. 3d) unveiled pronounced differences in the interactions that dictated the observed enantioselectivity. Non-covalent interaction (NCI) analysis[30] showed more pronounced π–π (Fig. 3e, highlighted by blue circles) and CH–π (Fig. 3e, highlighted by pink circles) interactions[40] between the 3,5-bis(trifluoromethyl)phenyl ring and one methyl group in the substrate with the two 9-anthranyl groups in the catalyst, respectively, in **TS-EF-2S** compared to **TS-EF-2R**.

Enantioselective hydroamination of other isolated unactivated alkene substrates

In order to clarify the impact of alkene substitution on the reaction, we subsequently explored the mechanisms of the enantioselective desymmetric hydroamination of distinctly substituted alkenes **AT-3–7** previously disclosed by some us (Table 1).[19c] Besides the hetero-ene pathway, we also considered the direct protonation mechanism by the catalyst for comparison. The results indicated consistently lower energy barriers for the hetero-ene pathway among all types of alkene substrates investigated (Fig. 4). Among all the alkenes, the barriers for the C2-disubstituted alkenes were generally lower than those for the C2-monosubsituted alkenes (**AT-5** *vs.* **AT-3** and **AT-6** *vs.* **AT-4**, respectively). Further natural population analysis (NPA) on both the starting materials and the corresponding transition states revealed the accumulation of significant positive atomic charges on the C2 carbons during the reactions of **AT-5** and **AT-6** but few charges for **AT-3** and **AT-4**. In particular, a discrete carbocation intermediate was successfully located only for **AT-5** with the lowest reaction barrier. Accordingly, the reactivity seemed to be primarily dictated by the capacity of the C2 substituents to stabilize transient carbocations. In contrast, the C1 substituents generally led to reaction retardation (**AT-3** *vs.* **AT-4** and **AT-5** *vs.* **AT-6**/**7**, respectively). In accordance with this reactivity trend, the C1-substitution without exception resulted in the decrease of innate alkene polarization in the starting materials, as evidenced by the computed atomic charges. As the alkene residues in the relevant transition states were highly polarized, the C1-substitution seemed to deactivate the alkenes for the formation of the corresponding transitions states, thus raising the reaction barriers. No remarkable steric clashes between these substitu-

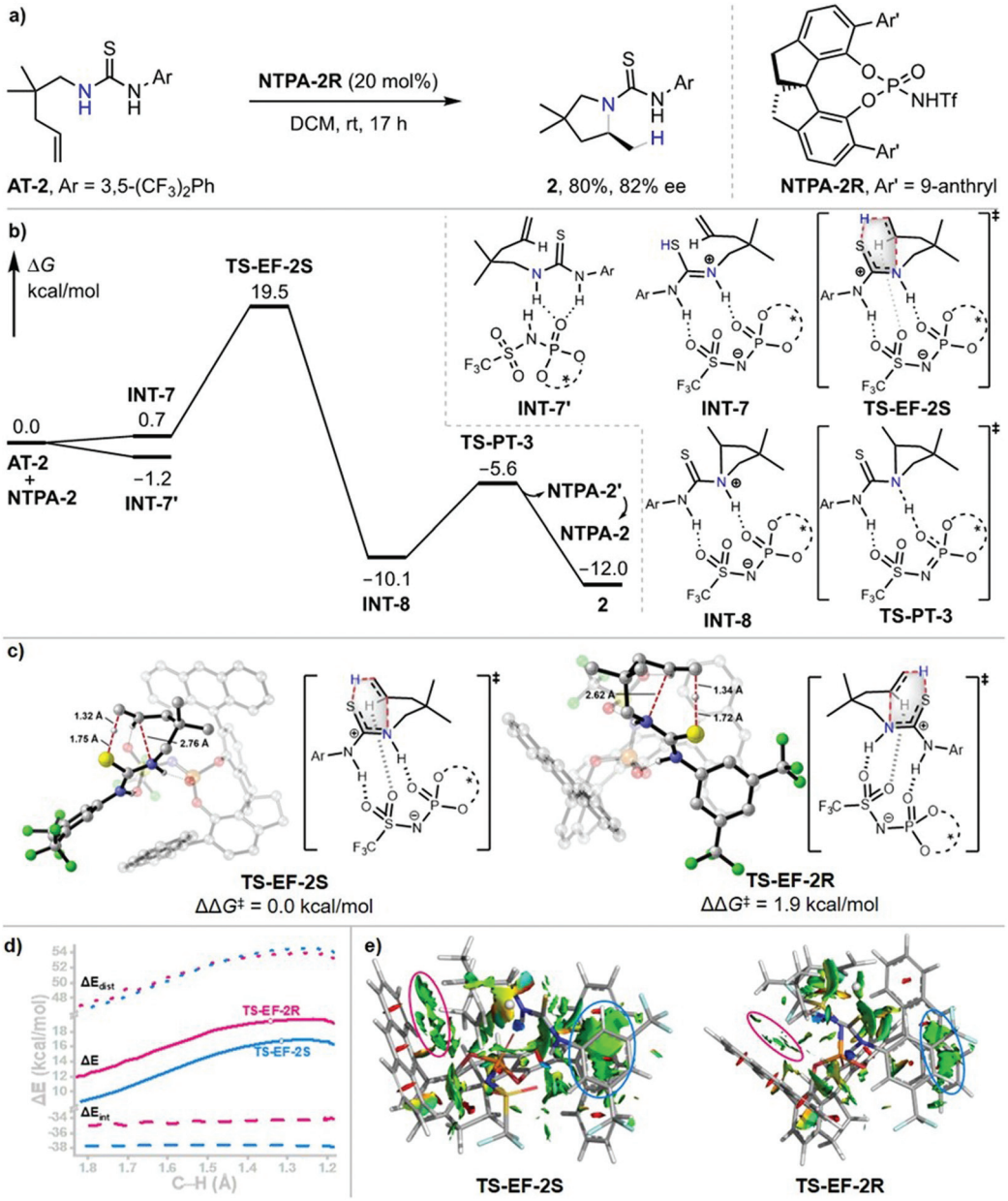

Fig. 3 Computational study on the hydroamination reaction of unactivated alkene substrate **AT-2**. (a) Experimental results of the hydroamination reaction of **AT-2** catalyzed by **NTPA-2R**. (b) Free energy profile of the hetero-ene reaction pathway. (c) Geometries and energies of the two optimized hetero-ene transition states leading to the two enantiomers of product **2**, respectively. (d) Distortion/interaction analysis on the enantioselective hetero-ene reaction step. (e) Color-filled NCI isosurfaces of the transition states **TS-EF-2S** and **TS-EF-2R** (blue, strong attraction; green, weak interaction; red, steric effect).

ents and the catalyst were observed in the pre-TS complexes and the corresponding transition states among these different alkene substrates (Fig. S9–S20†). These results are likely the unique benefits of the hetero-ene reaction mechanism for substrates bearing relatively small methyl substituents: the key rate-limiting proton transfer occurs in the peripheral region of the catalyst pocket, resulting in the reacting alkene being relatively far away from the sterically congested region of the catalyst.

Comparison with the chiral phosphoric acid catalyst

In comparison to **NTPA-2R**, the structurally similar chiral phosphoric acid (CPA) catalyst **CPA-1R** generally provided diminished yields and enantioselectivities (Fig. 5a).[19a] These results intrigued us and urged us to look into the mechanism behind the CPA-catalyzed hydroamination reaction. The acidity of CPAs is well known to be several orders of magnitude lower than that of NTPAs.[41] Consequently, we found that the

Table 1 Experimental results of different substituted alkenes

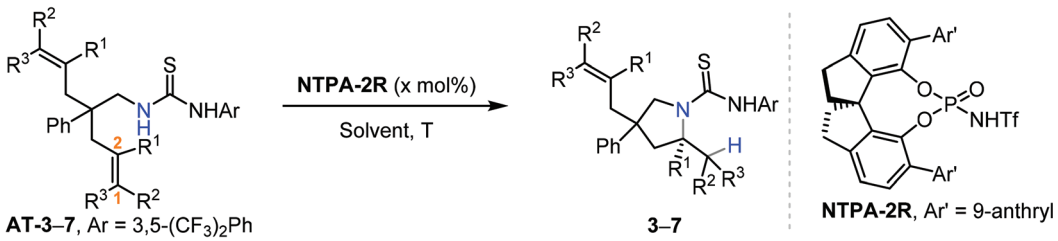

Compd. no.	R^1, R^2, R^3	Cat. loading/mol%	Solvent	Temp./°C	Yield/%
AT-3	H, H, H	15	*c*-Hexane	rt	82
AT-4	H, Me, H	30	*c*-Hexane	60	25
AT-5	Me, H, H	5	DCM	rt	83
AT-6	Me, Me, H	5	DCM	rt	86
AT-7	Me, Me, Me	20	DCM	rt	75

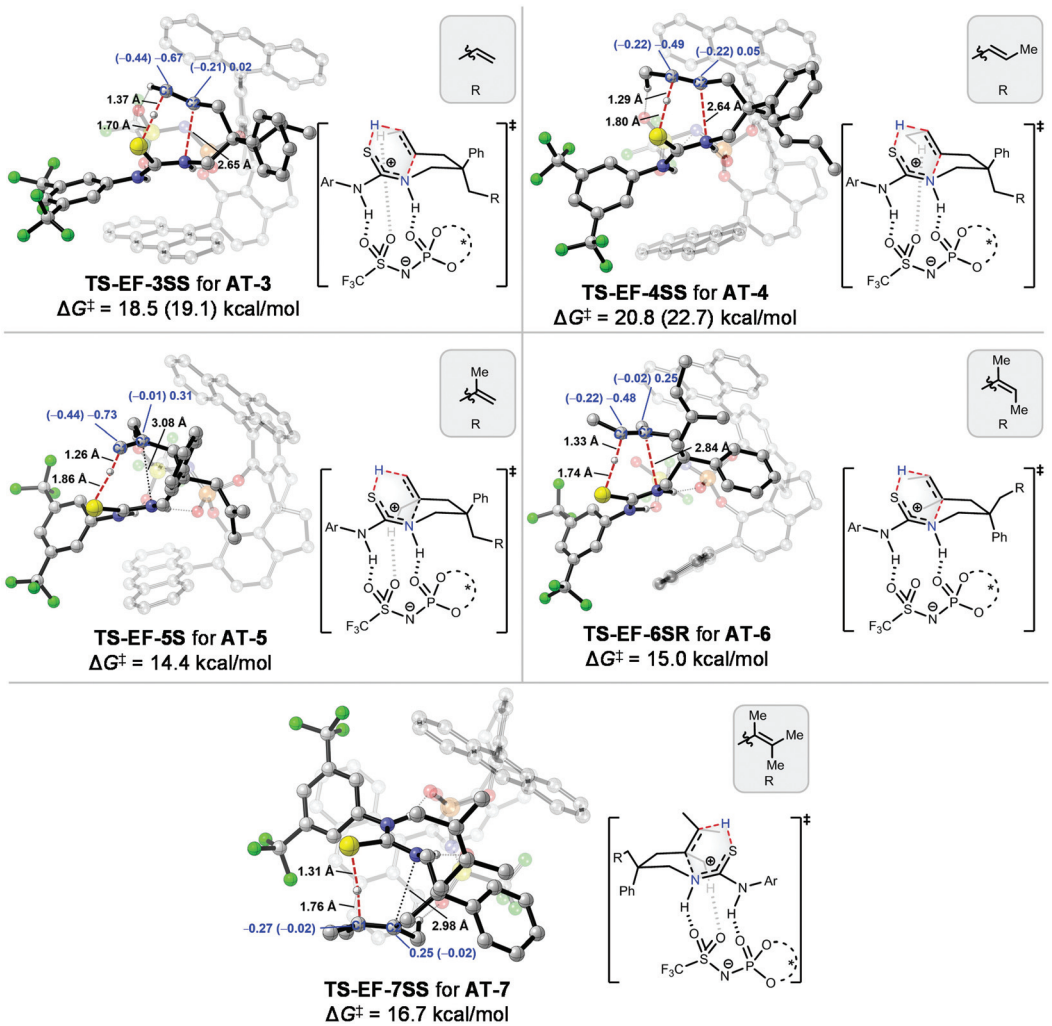

Fig. 4 Geometries and energies of the optimized hetero-ene transition states of various distinctly substituted isolated unactivated alkenes. Free activation energies for **AT-3** and **AT-4** shown in parentheses were calculated in cyclohexane at the same theory level for comparison. NPA charges on the alkenyl carbons in the transition states were shown as numbers in blue and those in the corresponding starting materials were shown in the following parentheses.

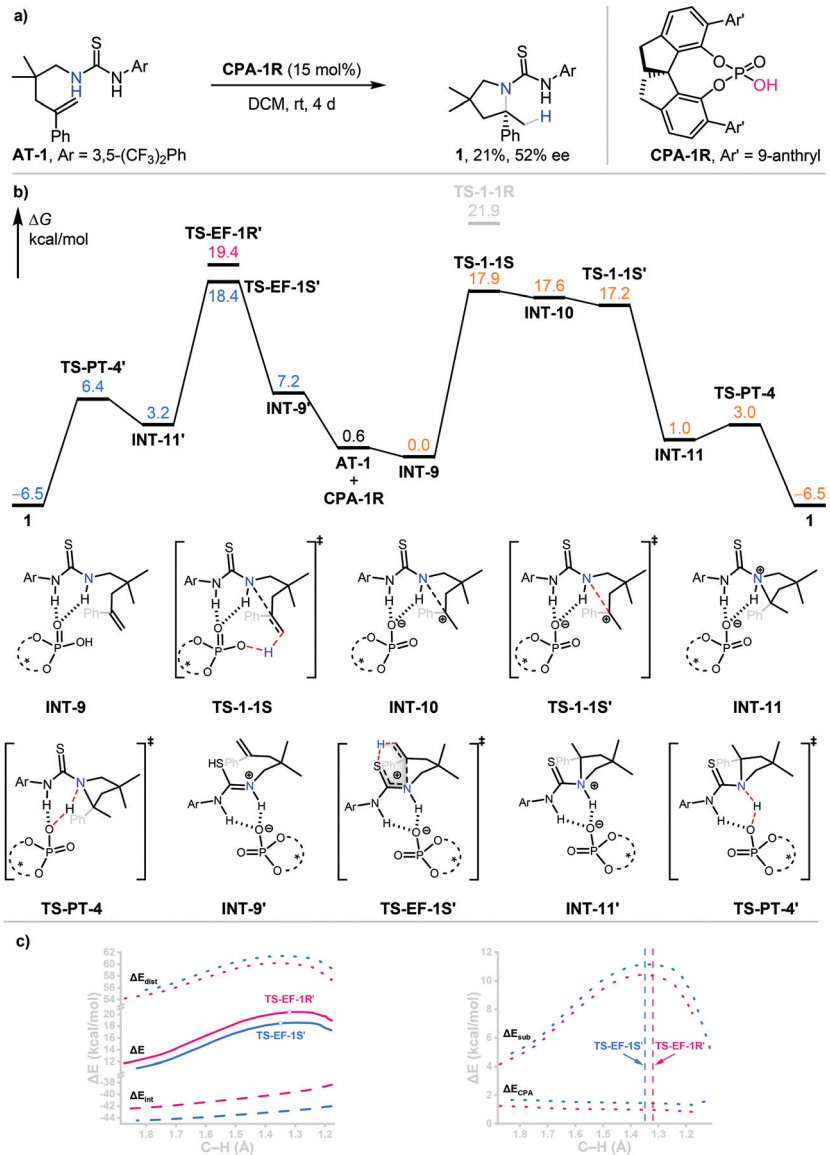

Fig. 5 Computational study on the hydroamination of **AT-1** catalyzed by **CPA-1R**. (a) Experimental results of the hydroamination reaction of **AT-1** catalyzed by **CPA-1R**. (b) Free energy profiles of the hetero-ene and the direct catalyst protonation pathways. (c) Distortion/interaction analysis on the enantioselective hetero-ene reaction step.

formation of the corresponding zwitterionic complex **INT9′** from **CPA-1R** and the substrate was much less thermodynamically favorable than that of the direct hydrogen-bonding complex **INT9** (Fig. 5b, ΔG = 7.2 kcal mol^{-1}). Nevertheless, the transition states **TS-EF-1S′** and **TS-1-1S** following **INT9′** and **INT9** along the hetero-ene and the direct catalyst protonation pathways, respectively, proved to be almost energetically equivalent. A concerted hetero-ene transition state **TS-EF-1S′** was located, while a transient carbocation intermediate **INT-10** was observed for the direct catalyst protonation pathway, with subsequent C–N bond formation *via* **TS-1-1S′**. Final proton transfers *via* **TS-PT-4′** and **TS-PT-4** were computed to be quite facile (ΔG_{act} = 3.2 and 2.0 kcal mol^{-1}, respectively) to afford the final product **1**. In this sense, the two pathways were competitively operating and the relative energies of the transition states **TS-1-1S/R** and **TS-EF-1S′/R′** determined the reactivity and enantioselectivity. Accordingly, the calculated reaction barriers, *i.e.*, 18.4 and 17.9 kcal mol^{-1} for the hetero-ene and the direct catalyst protonation pathways, respectively, are in good agreement with the experimentally observed low reactivity. In comparison to the same hetero-ene reaction catalyzed by **NTPA-2R**, the catalyst resting state changed from a protonated complex **INT-4** (Fig. S4 and S5†) to a hydrogen-bonded complex **INT-9** for the CPA-catalyzed reaction due to different catalyst acidities.[41] Consequently, a larger distortion for the transition state **TS-EF-1S′** resulted, compared to that for **TS-EF-1S** as both involved protonated substrates, which likely accounts for the

increased reaction barrier of the CPA-catalyzed hetero-ene reaction. As for the enantioselectivity, the observed moderate enantiomeric excess was mainly a result of the poorly enantioselective hetero-ene pathway with an unfavorable transition state **TS-EF-1R′** only 1.0 kcal mol^{-1} higher than **TS-EF-1S′** (1.5 kcal mol^{-1} higher than **TS-1-1S**). The subsequent distortion/interaction analysis concerning these two transition states revealed greatly diminished differences in distortion energies for the same reaction catalyzed by **NTPA-2R** (Fig. 5c, left). Further investigations on the distortions of the substrate and the catalyst fragments separately indicated a major loss of distortion differences on the catalyst parts (Fig. 5c, right), a result likely caused by the change in the relatively large NTf moiety in **NTPA-2R** compared to the sterically small OH group in **CPA-1R**.

Conclusions

In summary, we have computationally explored the mechanisms and origins of stereoselectivity for the enantioselective intramolecular hydroamination of isolated unactivated alkenes catalyzed by chiral *N*-triflylphosphoramide (NTPA) using DFT calculations. A rare hetero-ene reaction mechanism was revealed for a series of alkene substrates bearing different substitution patterns. Following an initial protonation of the thiourea moiety by the catalyst, the six-membered ring transition states of the hetero-ene reaction could proceed either in a stepwise or a concerted fashion, depending on the substitution patterns of the alkene moieties. A complex hydrogen bonding network between the catalyst and the substrate is present in the key transition states. Catalyst distortion controls the stereoselectivity for the styrene-type substrate, while noncovalent π interactions play a more important role in determining the stereoselectivity for alkenes with smaller methyl substituents. The different impacts of substituents on the internal or the terminal alkene carbons toward reactivity were due to their distinct influences on the polarization of alkene in transition states and the starting materials, respectively. By comparing the results with those for the chiral phosphoric acid (CPA)-catalyzed reaction, we reasoned that Brønsted acids with higher acidity favor the hetero-ene reaction, as a result of the facile formation of the protonated pre-TS complex. The results from our calculations indicate the potential involvement of uncommon pericyclic reaction mechanisms such as the hetero-ene reaction in the activation of alkenes by chiral Brønsted acid catalysis. This might serve as a promising yet underexplored strategy for the further development of challenging asymmetric hydrofunctionalization of unactivated alkenes.

Conflicts of interest

There are no conflicts to declare.

Acknowledgements

Financial support from the National Natural Science Foundation of China (No. 22171130 to P. Y.) and the Research Start-Up Funding of SZU (No. 8530300000137 and 860000002110230) is acknowledged. Computational work was supported by the Center for Computational Science and Engineering at Southern University of Science and Technology and the CHEM high-performance supercomputer cluster (CHEM-HPC) located at the Department of Chemistry, Southern University of Science and Technology. We thank Dr Yong-Feng Cheng, Zhang-Long Yu, Cong-Sheng Xu, and Dr Zhihan Zhang for helpful discussions.

References

1 For selected reviews, see: (*a*) G. Li, X. Huo, X. Jiang and W. Zhang, Asymmetric Synthesis of Allylic Compounds via Hydrofunctionalisation and Difunctionalisation of Dienes, Allenes, and Alkynes, *Chem. Soc. Rev.*, 2020, **49**, 2060–2118; (*b*) K. A. Margrey and D. A. Nicewicz, A General Approach to Catalytic Alkene Anti-Markovnikov Hydrofunctionalization Reactions via Acridinium Photoredox Catalysis, *Acc. Chem. Res.*, 2016, **49**, 1997–2006; (*c*) M. Rueping, D. Parmar and E. Sugiono, in *Asymmetric Brønsted Acid Catalysis*, ed. M. Rueping, D. Parmar and E. Sugiono, Wiley, Weinheim, 2016, ch. 6, pp. 161–182; (*d*) V. Rodriguez-Ruiz, R. Carlino, S. Bezzenine-Lafollee, R. Gil, D. Prim, E. Schulz and J. Hannedouche, Recent Developments in Alkene Hydro-Functionalisation Promoted by Homogeneous Catalysts Based on Earth Abundant Elements: Formation of C–N, C–O and C–P Bond, *Dalton Trans.*, 2015, **44**, 12029–12059; (*e*) *Hydrofunctionalization*, ed. V. P. Ananikov and M. Tanaka, Springer, Berlin, Heidelberg, 2013; (*f*) *Catalyc Heterofunctionalization*, ed. A. Togni and H. Grützmacher, Wiley, Weinheim, 2001.

2 For selected examples of alkene hydrofunctionalization with reagents other than common pronucleophiles, see: (*a*) J. Guo, Z. Cheng, J. Chen, X. Chen and Z. Lu, Iron- and Cobalt-Catalyzed Asymmetric Hydrofunctionalization of Alkenes and Alkynes, *Acc. Chem. Res.*, 2021, **54**, 2701–2716; (*b*) R. Y. Liu and S. L. Buchwald, CuH-Catalyzed Olefin Functionalization: From Hydroamination to Carbonyl Addition, *Acc. Chem. Res.*, 2020, **53**, 1229–1243; (*c*) D. K. Kim and V. M. Dong, in *Cobalt Catalysis in Organic Synthesis: Methods and Reactions*, ed. M. Hapke and G. Hilt, Wiley, Weinheim, 2020, ch. 3, pp. 67–88; (*d*) W. Ai, R. Zhong, X. Liu and Q. Liu, Hydride Transfer Reactions Catalyzed by Cobalt Complexes, *Chem. Rev.*, 2019, **119**, 2876–2953; (*e*) S. W. M. Crossley, C. Obradors, R. M. Martinez and R. A. Shenvi, Mn-, Fe-, and Co-Catalyzed Radical Hydrofunctionalizations of Olefins, *Chem. Rev.*, 2016, **116**, 8912–9000; (*f*) T. de Haro and C. Nevado, in *Comprehensive Organic Synthesis*, ed. P.

Knochel, Elsevier, Amsterdam, 2nd edn, 2014, pp. 1621–1659.

3 For selected reviews on chiral Brønsted acid catalysis, see: (*a*) Y.-B. Wang and B. Tan, Construction of Axially Chiral Compounds via Asymmetric Organocatalysis, *Acc. Chem. Res.*, 2018, **51**, 534–547; (*b*) C. Min and D. Seidel, Asymmetric Brønsted Acid Catalysis with Chiral Carboxylic Acids, *Chem. Soc. Rev.*, 2017, **46**, 5889–5902; (*c*) *Asymmetric Brønsted Acid Catalysis*, ed. M. Rueping, D. Parmar and E. Sugiono, Wiley, Weinheim, 2016; (*d*) T. Akiyama and K. Mori, Stronger Brønsted Acids: Recent Progress, *Chem. Rev.*, 2015, **115**, 9277–9306; (*e*) T. James, M. van Gemmeren and B. List, Development and Applications of Disulfonimides in Enantioselective Organocatalysis, *Chem. Rev.*, 2015, **115**, 9388–9409; (*f*) Z. Wang, Z. Chen and J. Sun, Catalytic Asymmetric Nucleophilic Openings of 3-Substituted Oxetanes, *Org. Biomol. Chem.*, 2014, **12**, 6028–6032; (*g*) D. Parmar, E. Sugiono, S. Raja and M. Rueping, Complete Field Guide to Asymmetric BINOL-Phosphate Derived Brønsted Acid and Metal Catalysis: History and Classification by Mode of Activation; Brønsted Acidity, Hydrogen Bonding, Ion Pairing, and Metal Phosphates, *Chem. Rev.*, 2014, **114**, 9047–9153; (*h*) J. Yu, F. Shi and L.-Z. Gong, Brønsted-Acid-Catalyzed Asymmetric Multicomponent Reactions for the Facile Synthesis of Highly Enantioenriched Structurally Diverse Nitrogenous Heterocycles, *Acc. Chem. Res.*, 2011, **44**, 1156–1171; (*i*) M. Terada, Chiral Phosphoric Acids as Versatile Catalysts for Enantioselective Transformations, *Synthesis*, 2010, 1929–1982; (*j*) S.-L. You, Q. Cai and M. Zeng, Chiral Brønsted Acid Catalyzed Friedel–Crafts Alkylation Reactions, *Chem. Soc. Rev.*, 2009, **38**, 2190–2201; (*k*) D. Kampen, C. M. Reisinger and B. List, in *Asymmetric Organocatalysis*, ed. B. List, Springer, Berlin, Heidelberg, 2010, pp. 395–456.

4 For selected examples, see: (*a*) H. J. Lucas and W. F. Eberz, The Hydration of Unsaturated Compounds. I. The Hydration Rate of Isobutene in Dilute Nitric Acid, *J. Am. Chem. Soc.*, 1934, **56**, 460–464; (*b*) B. Schlummer and J. F. Hartwig, Brønsted Acid-Catalyzed Intramolecular Hydroamination of Protected Alkenylamines. Synthesis of Pyrrolidines and Piperidines, *Org. Lett.*, 2002, **4**, 1471–1474; (*c*) Z. Li, J. Zhang, C. Brouwer, C.-G. Yang, N. W. Reich and C. He, Brønsted Acid Catalyzed Addition of Phenols, Carboxylic Acids, and Tosylamides to Simple Olefins, *Org. Lett.*, 2006, **8**, 4175–4178 For a selected review on this topic, see: (*d*) H. Yamamoto and D. Nakashima, in *Acid Catalysis in Modern Organic Synthesis*, ed. H. Yamamoto and K. Ishihara, Wiley, Weinheim, 2008, ch. 1, vol. 1, pp. 35–62.

5 (*a*) L. Ackermann and A. Althammer, Phosphoric Acid Diesters as Efficient Catalysts for Hydroaminations of Nonactivated Alkenes and an Application to Asymmetric Hydroaminations, *Synlett*, 2008, 995–998; (*b*) G.-Q. Liu, B. Cui, H. Sun and Y.-M. Li, Trifluoroacetic Acid-Promoted Intramolecular Hydroamination of Unfunctionalized Olefins Bearing Electron-Rich Amino Groups, *Tetrahedron*, 2014, **70**, 5696–5703.

6 P. F. Vlad, Superacidic Cyclization of Terpenoids, *Pure Appl. Chem.*, 1993, **65**, 1329–1336.

7 For early examples, see: (*a*) K. Ishihara, S. Nakamura and H. Yamamoto, The First Enantioselective Biomimetic Cyclization of Polyprenoids, *J. Am. Chem. Soc.*, 1999, **121**, 4906–4907; (*b*) S. Nakamura, K. Ishihara and H. Yamamoto, Enantioselective Biomimetic Cyclization of Isoprenoids Using Lewis Acid-Assisted Chiral Brønsted Acids: Abnormal Claisen Rearrangements and Successive Cyclizations, *J. Am. Chem. Soc.*, 2000, **122**, 8131–8140; (*c*) K. Ishihara, H. Ishibashi and H. Yamamoto, Enantioselective Biomimetic Cyclization of Homo(polyprenyl)arenes. A New Entry to (+)-Podpcarpa-8,11,13-triene Diterpenoids and (−)-Tetracyclic Polyprenoid of Sedimentary Origin, *J. Am. Chem. Soc.*, 2001, **123**, 1505–1506 For a review on this topic, see: (*d*) H. Yamamoto and K. Futatsugi, "Designer Acids": Combined Acid Catalysis for Asymmetric Synthesis, *Angew. Chem., Int. Ed.*, 2005, **44**, 1924–1942.

8 (*a*) A. Sakakura, M. Sakuma and K. Ishihara, Chiral Lewis Base-Assisted Brønsted Acid (LBBA)-Catalyzed Enantioselective Cyclization of 2-Geranylphenols, *Org. Lett.*, 2011, **13**, 3130–3133; (*b*) M. Sakuma, A. Sakakura and K. Ishihara, Kinetic Resolution of Racemic Carboxylic Acids through Asymmetric Protolactonization Promoted by Chiral Phosphonous Acid Diester, *Org. Lett.*, 2013, **15**, 2838–2841 For a review on LBBA, see: (*c*) X.-P. Zeng and J. Zhou, in *Multicatalyst System in Asymmetric Catalysis*, ed. J. Zhou, Wiley, Hoboken, New Jersey, 2014, ch. 6, pp. 411–474.

9 (*a*) N. Tsuji, J. L. Kennemur, T. Buyck, S. Lee, S. Prévost, P. S. J. Kaib, D. Bykov, C. Farès and B. List, Activation of Olefins via Asymmetric Brønsted Acid Catalysis, *Science*, 2018, **359**, 1501–1505; (*b*) P. Zhang, N. Tsuji, J. Ouyang and B. List, Strong and Confined Acids Catalyze Asymmetric Intramolecular Hydroarylations of Unactivated Olefins with Indoles, *J. Am. Chem. Soc.*, 2021, **143**, 675–680 For a review on IDPi, see: (*c*) L. Schreyer, R. Properzi and B. List, IDPi Catalysis, *Angew. Chem., Int. Ed.*, 2019, **58**, 12761–12777.

10 For chiral Brønsted acid-catalyzed asymmetric hydrofunctionalization of only conjugated alkenes, see: (*a*) N. D. Shapiro, V. Rauniyar, G. L. Hamilton, J. Wu and F. D. Toste, Asymmetric Additions to Dienes Catalysed by a Dithiophosphoric Acid, *Nature*, 2011, **470**, 245–249; (*b*) J. Kikuchi and M. Terada, Enantioselective Addition Reaction of Azlactones with Styrene Derivatives Catalyzed by Strong Chiral Brønsted Acids, *Angew. Chem., Int. Ed.*, 2019, **58**, 8458–8462.

11 For selected reviews on asymmetric ion-pairing catalysis, see: (*a*) J. Kikuchi and M. Terada, Enantioconvergent Substitution Reactions of Racemic Electrophiles by Organocatalysis, *Chem. – Eur. J.*, 2021, **27**, 10215–10225; (*b*) C.-W. Lei, B.-S. Mu, F. Zhou, J.-S. Yu, Y. Zhou and J. Zhou, Organocatalytic Enantioselective Reactions Involving Prochiral Carbocationic Intermediates, *Chem.*

Commun., 2021, **57**, 9178–9191; (*c*) X. Zhang and C.-H. Tan, Stereospecific and Stereoconvergent Nucleophilic Substitution Reactions at Tertiary Carbon Centers, *Chem*, 2021, **7**, 1451–1486; (*d*) D. Qian and J. Sun, Recent Progress in Asymmetric Ion-Pairing Catalysis with Ammonium Salts, *Chem. – Eur. J.*, 2019, **25**, 3740–3751; (*e*) L. Zong and C.-H. Tan, Phase-Transfer and Ion-Pairing Catalysis of Pentanidiums and Bisguanidiniums, *Acc. Chem. Res.*, 2017, **50**, 842–856; (*f*) M. Jia and M. Bandini, Counterion Effects in Homogeneous Gold Catalysis, *ACS Catal.*, 2015, **5**, 1638–1652; (*g*) M. Waser, J. Novacek and K. Gratzer, in *Cooperative Catalysis: Designing Efficient Catalysts for Synthesis*, ed. R. Peters, Wiley, Weinheim, 2015, ch. 7, pp. 197–226; (*h*) K. Brak and E. N. Jacobsen, Asymmetric Ion-Pairing Catalysis, *Angew. Chem., Int. Ed.*, 2013, **52**, 534–561; (*i*) M. Mahlau and B. List, Asymmetric Counteranion-Directed Catalysis: Concept, Definition, and Applications, *Angew. Chem., Int. Ed.*, 2013, **52**, 518–533; (*j*) R. J. Phipps, G. L. Hamilton and F. D. Toste, The Progression of Chiral Anions fom Concepts to Applications in Asymmetric Catalysis, *Nat. Chem.*, 2012, **4**, 603–614.

12 A. R. Brown, C. Uyeda, C. A. Brotherton and E. N. Jacobsen, Enantioselective Thiourea-Catalyzed Intramolecular Cope-Type Hydroamination, *J. Am. Chem. Soc.*, 2013, **135**, 6747–6749.

13 For selected reviews on chiral thiourea catalysis, see: (*a*) T. Parvin, R. Yadav and L. H. Choudhury, Recent Applications of Thiourea-Based Organocatalysts in Asymmetric Multicomponent Reactions (AMCRs), *Org. Biomol. Chem.*, 2020, **18**, 5513–5532; (*b*) F. Steppeler, D. Iwan, E. Wojaczyńska and J. Wojaczyński, Chiral Thioureas—Preparation and Significance in Asymmetric Synthesis and Medicinal Chemistry, *Molecules*, 2020, **25**, 401; (*c*) M. C. Gimeno and R. P. Herrera, Hydrogen Bonding and Internal or External Lewis or Brønsted Acid Assisted (Thio)urea Catalysts, *Eur. J. Org. Chem.*, 2020, 1057–1068; (*d*) D. Limnios and C. G. Kokotos, in *Sustainable Catalysis: Without Metals or Other Endangered Elements, Part 2*, The Royal Society of Chemistry, 2016, ch. 19, pp. 196–255; (*e*) X. Fang and C.-J. Wang, Recent Advances in Asymmetric Organocatalysis Mediated by Bifunctional Amine–Thioureas Bearing Multiple Hydrogen-Bonding Donors, *Chem. Commun.*, 2015, **51**, 1185–1197; (*f*) M. Kotke and P. R. Schreiner, in *Hydrogen Bonding in Organic Synthesis*, ed. P. M. Pihko, Wiley, Weinheim, 2009, ch. 6, pp. 141–351; (*g*) S. J. Connon, Organocatalysis Mediated by (Thio)urea Derivatives, *Chem. – Eur. J.*, 2006, **12**, 5418–5427.

14 For selected reviews on hydrogen-bond catalysis, see: (*a*) H. Miyabe, in *Recent Advances in Organocatalysis*, ed. I. Karame and H. Srour, ExLi4EvA, 2016, ch. 1; (*b*) M. Žabka and R. Šebesta, Experimental and Theoretical Studies in Hydrogen-Bonding Organocatalysis, *Molecules*, 2015, **20**, 15500–15524; (*c*) X. Lu and L. Deng, in *Cooperative Catalysis: Designing Efficient Catalysts for Synthesis*, ed. R. Peters, Wiley, Weinheim, 2015, ch. 5, pp. 145–170; (*d*) *Hydrogen Bonding in Organic Synthesis*, ed. P. M. Pihko, Wiley, Weinheim, 2009; (*e*) A. G. Doyle and E. N. Jacobsen, Small-Molecule H-Bond Donors in Asymmetric Catalysis, *Chem. Rev.*, 2007, **107**, 5713–5743; (*f*) M. S. Taylor and E. N. Jacobsen, Asymmetric Catalysis by Chiral Hydrogen-Bond Donors, *Angew. Chem., Int. Ed.*, 2006, **45**, 1520–1543; (*g*) P. R. Schreiner, Metal-Free Organocatalysis through Explicit Hydrogen Bonding Interactions, *Chem. Soc. Rev.*, 2003, **32**, 289–296.

15 N. J. Cooper and D. W. Knight, The Reverse Cope Cyclisation: A Classical Reaction Goes Backwards, *Tetrahedron*, 2004, **60**, 243–269.

16 For other asymmetric hydroamination reactions via a Cope-type reaction mechanism, see: (*a*) M. Zhang, S. Liu, H. Li, Y. Guo, N. Li, M. Guan, H. Mehfooz, J. Zhao and Q. Zhang, Copper-Catalyzed Cope-Type Hydroamination of Nonactivated Olefins toward Cyclic Nitrones: Scope, Mechanism, and Enantioselective Process Development, *Chem. – Eur. J.*, 2019, **25**, 12620–12627; (*b*) Z. Li, J. Zhao, B. Sun, T. Zhou, M. Liu, S. Liu, M. Zhang and Q. Zhang, Asymmetric Nitrone Synthesis via Ligand-Enabled Copper-Catalyzed Cope-Type Hydroamination of Cyclopropene with Oxime, *J. Am. Chem. Soc.*, 2017, **139**, 11702–11705; (*c*) M. J. MacDonald, C. R. Hesp, D. J. Schipper, M. Pesant and A. M. Beauchemin, Highly Enantioselective Intermolecular Hydroamination of Allylic Amines with Chiral Aldehydes as Tethering Catalysts, *Chem. – Eur. J.*, 2013, **19**, 2597–2601; (*d*) M. J. MacDonald, D. J. Schipper, P. J. Ng, J. Moran and A. M. Beauchemin, A Catalytic Tethering Strategy: Simple Aldehydes Catalyze Intermolecular Alkene Hydroaminations, *J. Am. Chem. Soc.*, 2011, **133**, 20100–20103.

17 B.-J. Li, C. Ei-Nachef and A. M. Beauchemin, Organocatalysis Using Aldehydes: The Development and Improvement of Catalytic Hydroaminations, Hydrations and Hydrolyses, *Chem. Commun.*, 2017, **53**, 13192–13204.

18 For selected reviews on asymmetric hydroamination, see: (*a*) L. Rocard, D. Chen, A. Stadler, H. Zhang, R. Gil, S. Bezzenine and J. Hannedouche, Earth-Abundant 3d Transition Metal Catalysts for Hydroalkoxylation and Hydroamination of Unactivated Alkenes, *Catalysts*, 2021, **11**, 674; (*b*) C. Michon, M.-A. Abadie, F. Medina and F. Agbossou-Niedercorn, Recent Metal-Catalysed Asymmetric Hydroaminations of Alkenes, *J. Organomet. Chem.*, 2017, **847**, 13–27; (*c*) E. Bernoud, C. Lepori, M. Mellah, E. Schulz and J. Hannedouche, Recent Advances in Metal Free- and Late Transition Metal-Catalysed Hydroamination of Unactivated Alkenes, *Catal. Sci. Technol.*, 2015, **5**, 2017–2037; (*d*) L. Huang, M. Arndt, K. Gooßen, H. Heydt and L. J. Gooßen, Late Transition Metal-Catalyzed Hydroamination and Hydroamidation, *Chem. Rev.*, 2015, **115**, 2596–2697; (*e*) J. Hannedouche and E. Schulz, Asymmetric Hydroamination: A Survey of the Most Recent Developments, *Chem. – Eur. J.*, 2013, **19**, 4972–4985; (*f*) S. R. Chemler, The Enantioselective Intramolecular Aminative Functionalization of Unactivated

Alkenes, Dienes, Allenes and Alkynes for the Synthesis of Chiral Nitrogen Heterocycles, *Org. Biomol. Chem.*, 2009, **7**, 3009–3019; (*g*) T. E. Müller, K. C. Hultzsch, M. Yus, F. Foubelo and M. Tada, Hydroamination: Direct Addition of Amines to Alkenes and Alkynes, *Chem. Rev.*, 2008, **108**, 3795–3892; (*h*) J. J. Brunet and D. Neibecker, in *Catalyc Heterofunctionalization*, ed. A. Togni and H. Grützmacher, Wiley, Weinheim, 2001, ch. 4, pp. 91–141.

19 (*a*) J.-S. Lin, P. Yu, L. Huang, P. Zhang, B. Tan and X.-Y. Liu, Brønsted Acid Catalyzed Asymmetric Hydroamination of Alkenes: Synthesis of Pyrrolidines Bearing a Tetrasubstituted Carbon Stereocenter, *Angew. Chem., Int. Ed.*, 2015, **54**, 7847–7851; (*b*) J.-S. Lin, T.-T. Li, G.-Y. Jiao, Q.-S. Gu, J.-T. Cheng, L. Lv and X.-Y. Liu, Chiral Brønsted Acid Catalyzed Dynamic Kinetic Asymmetric Hydroamination of Racemic Allenes and Asymmetric Hydroamination of Dienes, *Angew. Chem., Int. Ed.*, 2019, **58**, 7092–7096; (*c*) Z.-L. Yu, Y.-F. Cheng, N.-C. Jiang, J. Wang, L.-W. Fan, Y. Yuan, Z.-L. Li, Q.-S. Gu and X.-Y. Liu, Desymmetrization of Unactivated Bis-Alkenes via Chiral Brønsted Acid-Catalysed Hydroamination, *Chem. Sci.*, 2020, **11**, 5987–5993.

20 For a recent related asymmetric hydroamination reaction catalyzed by chiral disulfonimide catalysts, see: R. Takagi, D. T. Duong and T. Ichiki, Disulfonimide Catalyzed Asymmetric Intramolecular Hydroamination of Alkenyl Thioureas: Concentration Effect in the Hydroamination, *Tetrahedron*, 2021, **94**, 132332.

21 For recently disclosed theoretical studies on asymmetric hydroamination reactions of dienes, allenes, and styrenes during the preparation of this article, see ref. 20 and: (*a*) Y. Qiu, H. Yuan, X. Zhang and J. Zhang, Insights into the Chiral Phosphoric Acid-Catalyzed Dynamic Kinetic Asymmetric Hydroamination of Racemic Allenes: An Allyl Carbocation/Phosphate Pair Mechanism, *J. Org. Chem.*, 2021, **86**, 4121–4130; (*b*) R. Takagi and D. T. Duong, Computational Study on *N*-Triflylphosphoramide-Catalyzed Enantioselective Hydroamination of Alkenyl Thiourea, *Org. Biomol. Chem.*, 2021, **19**, 8806–8811.

22 (*a*) D. Nakashima and H. Yamamoto, Design of Chiral *N*-Triflyl Phosphoramide as a Strong Chiral Brønsted Acid and Its Application to Asymmetric Diels–Alder Reaction, *J. Am. Chem. Soc.*, 2006, **128**, 9626–9627; (*b*) G. Caballero-García and J. M. Goodman, *N*-Triflylphosphoramides: Highly Acidic Catalysts for Asymmetric Transformations, *Org. Biomol. Chem.*, 2021, **19**, 9565–9618.

23 M. J. Frisch, G. W. Trucks, H. B. Schlegel, G. E. Scuseria, M. A. Robb, J. R. Cheeseman, G. Scalmani, V. Barone, G. A. Petersson, H. Nakatsuji, X. Li, M. Caricato, A. V. Marenich, J. Bloino, B. G. Janesko, R. Gomperts, B. Mennucci, H. P. Hratchian, J. V. Ortiz, A. F. Izmaylov, J. L. Sonnenberg, D. Williams-Young, F. Ding, F. Lipparini, F. Egidi, J. Goings, B. Peng, A. Petrone, T. Henderson, D. Ranasinghe, V. G. Zakrzewski, J. Gao, N. Rega, G. Zheng, W. Liang, M. Hada, M. Ehara, K. Toyota, R. Fukuda, J. Hasegawa, M. Ishida, T. Nakajima, Y. Honda, O. Kitao, H. Nakai, T. Vreven, K. Throssell, J. A. Montgomery Jr., J. E. Peralta, F. Ogliaro, M. J. Bearpark, J. J. Heyd, E. N. Brothers, K. N. Kudin, V. N. Staroverov, T. A. Keith, R. Kobayashi, J. Normand, K. Raghavachari, A. P. Rendell, J. C. Burant, S. S. Iyengar, J. Tomasi, M. Cossi, J. M. Millam, M. Klene, C. Adamo, R. Cammi, J. W. Ochterski, R. L. Martin, K. Morokuma, O. Farkas, J. B. Foresman and D. J. Fox, *Gaussian 16, Revision A.03*, Gaussian, Inc., Wallingford, CT, 2016.

24 (*a*) P. Pracht, F. Bohle and S. Grimme, Automated Exploration of the Low-Energy Chemical Space with Fast Quantum Chemical Methods, *Phys. Chem. Chem. Phys.*, 2020, **22**, 7169–7192; (*b*) S. Grimme, Exploration of Chemical Compound, Conformer, and Reaction Space with Meta-Dynamics Simulations Based on Tight-Binding Quantum Chemical Calculations, *J. Chem. Theory Comput.*, 2019, **15**, 2847–2862.

25 (*a*) C. Lee, W. Yang and R. G. Parr, Development of the Colle-Salvetti Correlation-Energy Formula into a Functional of the Electron Density, *Phys. Rev. B: Condens. Matter Mater. Phys.*, 1988, **37**, 785–789; (*b*) A. D. Becke, Density–Functional Thermochemistry. III. The Role of Exact Exchange, *J. Chem. Phys.*, 1993, **98**, 5648–5652; (*c*) P. J. Stephens, F. J. Devlin, C. F. Chabalowski and M. J. Frisch, *Ab Initio* Calculation of Vibrational Absorption and Circular Dichroism Spectra Using Density Functional Force Fields, *J. Phys. Chem.*, 1994, **98**, 11623–11627; (*d*) J. Zhang, P. Yu, S.-Y. Li, H. Sun, S.-H. Xiang, J. Wang, K. N. Houk and B. Tan, Asymmetric Phosphoric Acid–Catalyzed Four-Component Ugi Reaction, *Science*, 2018, **361**, eaas8707.

26 Y. Zhao and D. G. Truhlar, The M06 Suite of Density Functionals for Main Group Thermochemistry, Thermochemical Kinetics, Noncovalent Interactions, Excited States, and Transition Elements: Two New Functionals and Systematic Testing of Four M06-Class Functionals and 12 Other Functionals, *Theor. Chem. Acc.*, 2008, **120**, 215–241.

27 A. V. Marenich, C. J. Cramer and D. G. Truhlar, Universal Solvation Model Based on Solute Electron Density and on a Continuum Model of the Solvent Defined by the Bulk Dielectric Constant and Atomic Surface Tensions, *J. Phys. Chem. B*, 2009, **113**, 6378–6396.

28 (*a*) S. Grimme, J. Antony, S. Ehrlich and H. Krieg, A Consistent and Accurate *Ab Initio* Parametrization of Density Functional Dispersion Correction (DFT-D) for the 94 Elements H-Pu, *J. Chem. Phys.*, 2010, **132**, 154104; (*b*) S. Grimme, S. Ehrlich and L. Goerigk, Effect of the Damping Function in Dispersion Corrected Density Functional Theory, *J. Comput. Chem.*, 2011, **32**, 1456–1465.

29 J.-D. Chai and M. Head-Gordon, Long-Range Corrected Hybrid Density Functionals with Damped Atom–Atom Dispersion Corrections, *Phys. Chem. Chem. Phys.*, 2008, **10**, 6615–6620.

30 (*a*) E. R. Johnson, S. Keinan, P. Mori-Sánchez, J. Contreras-García, A. J. Cohen and W. Yang, Revealing Noncovalent

Interactions, *J. Am. Chem. Soc.*, 2010, **132**, 6498–6506; (*b*) J. Contreras-García, E. R. Johnson, S. Keinan, R. Chaudret, J.-P. Piquemal, D. N. Beratan and W. Yang, NCIPLOT: A Program for Plotting Noncovalent Interaction Regions, *J. Chem. Theory Comput.*, 2011, **7**, 625–632; (*c*) R. Laplaza, F. Peccati, D. Arias-Olivares and J. Contreras-García, in *Complementary Bonding Analysis*, ed. G. Simon, De Gruyter, 2021, ch. 14, pp. 353–378.

31 T. Lu and F. Chen, Multiwfn: A Multifunctional Wavefunction Analyzer, *J. Comput. Chem.*, 2012, **33**, 580–592.

32 *The PyMOL Molecular Graphics System, version 2.5.2*, Schrödinger, LLC.

33 (*a*) I. Fernández and F. M. Bickelhaupt, The Activation Strain Model and Molecular Orbital Theory: Understanding and Designing Chemical Reactions, *Chem. Soc. Rev.*, 2014, **43**, 4953–4967; (*b*) L. P. Wolters and F. M. Bickelhaupt, The Activation Strain Model and Molecular Orbital Theory, *Wiley Interdiscip. Rev.: Comput. Mol. Sci.*, 2015, **5**, 324–343; (*c*) F. M. Bickelhaupt and K. N. Houk, Analyzing Reaction Rates with the Distortion/Interaction-Activation Strain Model, *Angew. Chem., Int. Ed.*, 2017, **56**, 10070–10086.

34 (*a*) A. E. Reed, R. B. Weinstock and F. Weinhold, Natural population analysis, *J. Chem. Phys.*, 1985, **83**, 735–746; (*b*) A. E. Reed, L. A. Curtiss and F. Weinhold, Intermolecular interactions from a natural bond orbital, donor–acceptor viewpoint, *Chem. Rev.*, 1988, **88**, 899–926; (*c*) E. D. Glendening, A. E. Reed, J. E. Carpenter and F. Weinhold, *NBO 3.0*, Theoretical Chemistry Institute, University of Wisconsin, Madison, Wisconsin, 1990.

35 C. Y. Legault, *CYLview, 1.0b*, Universitéde Sherbrooke, 2009 (http://www.cylview.org).

36 (*a*) J. P. Lovie-Toon, C. M. Tram, B. L. Flynn and E. H. Krenske, Mechanisms of Carbonyl Activation by BINOL *N*-Triflylphosphoramides: Enantioselective Nazarov Cyclizations, *ACS Catal.*, 2017, **7**, 3466–3476; (*b*) X. Hong, H. B. Küçük, M. S. Maji, Y.-F. Yang, M. Rueping and K. N. Houk, Mechanism and Selectivity of *N*-Triflylphosphoramide Catalyzed ($3^+ + 2$) Cycloaddition between Hydrazones and Alkenes, *J. Am. Chem. Soc.*, 2014, **136**, 13769–13780.

37 For selected reviews, see: (*a*) E.-Z. Lin, Y. Xu, K. Ji and L.-W. Ye, Recent Advances towards Catalytic Asymmetric Conia-Ene-Type Reactions, *Chin. Chem. Lett.*, 2021, **32**, 954–962; (*b*) D. Hack, M. Blümel, P. Chauhan, A. R. Philipps and D. Enders, Catalytic Conia-ene and Related Reactions, *Chem. Soc. Rev.*, 2015, **44**, 6059–6093.

38 For selected reviews, see: (*a*) X. Liu, K. Zheng and X. Feng, Advancements in Catalytic Asymmetric Intermolecular Ene-Type Reactions, *Synthesis*, 2014, 2241–2257; (*b*) K. Mikami and M. Shimizu, Asymmetric Ene Reactions in Organic Synthesis, *Chem. Rev.*, 1992, **92**, 1021–1050; (*c*) W. Oppolzer and V. Snieckus, Intramolecular Ene Reactions in Organic Synthesis, *Angew. Chem., Int. Ed. Engl.*, 1978, **17**, 476–486; (*d*) H. M. R. Hoffmann, The Ene Reaction, *Angew. Chem., Int. Ed. Engl.*, 1969, **8**, 556–577.

39 For a related hetero-ene reaction, see: M.-A. Chiacchio, L. Legnani, P. Caramella, T. Tejero and P. Merino, Revealing Carbocations in Highly Asynchronous Concerted Reactions: The Ene-Type Reaction between Dithiocarboxylic Acids and Alkenes, *Tetrahedron*, 2018, **74**, 5627–5634.

40 (*a*) R. Maji and S. E. Wheeler, in *Aromatic Interactions: Frontiers in Knowledge and Application*, ed. D. W. Johnson and F. Hof, The Royal Society of Chemistry, 2017, ch. 2, pp. 18–38; (*b*) A. J. Neel, M. J. Hilton, M. S. Sigman and F. D. Toste, Exploiting Non-Covalent π Interactions for Catalyst Design, *Nature*, 2017, **543**, 637–646; (*c*) E. H. Krenske and K. N. Houk, Aromatic Interactions as Control Elements in Stereoselective Organic Reactions, *Acc. Chem. Res.*, 2013, **46**, 979–989.

41 K. Kaupmees, N. Tolstoluzhsky, S. Raja, M. Rueping and I. Leito, On the Acidity and Reactivity of Highly Effective Chiral Brønsted Acid Catalysts: Establishment of an Acidity Scale, *Angew. Chem., Int. Ed.*, 2013, **52**, 11569–11572.